Yu, S., Zhang, M., Hong, Q., Sato, E., & Antoniou, I. (2026). Coordinated differential protection for multimode operation in a future spherical tokamak fusion power plant. IEEE Transactions on Plasma Science, 1-7. https://doi.org/10.1109/tps.2026.3693938. For the purpose of open access, a CC BY 4.0 licence has been applied

Coordinated Differential Protection for Multimode Operation in a Future Spherical Tokamak Fusion Power Plant

Shiyao Yu, *Graduate Student Member, IEEE*, Min Zhang, *Senior Member, IEEE*, Qiteng Hong, *Senior Member, IEEE*, Eduardo Sato, and Ioannis Antoniou

***Abstract*—Commercial deployment of the Spherical Tokamak for Energy Production (STEP) requires a reliable protection philosophy for its prototype power plant to prevent system faults from damaging reactor-related components. However, relay protection for the STEP prototype power plant (SPP) microgrid has not yet been specifically addressed. This article develops a coordinated differential protection scheme tailored to the SPP's multimode operation and hybrid sources. The scheme augments slope-biased current differential protection with a phase-angle-superimposed term derived from two-terminal phasors and employs current restraint for inrush-related disturbances and time synchronization mismatch. Mode-dependent bias curves and pickup thresholds are used to accommodate bidirectional power flow and changing fault levels. The scheme is evaluated on an RTDS/RSCAD model based on U.K. Fusion Energy (UKFE) SPP data, U.K. Grid Code provisions, and IAEA Safety Standards No. SSG-34 credible fault scenarios, covering multiple fault types, locations, impedances, and operating modes. Compared with conventional slope-biased differential protection, the proposed scheme improves the detection of high-impedance internal faults while maintaining external-fault restraint. These results address a protection gap for fusion power plants and support the grid-facing viability of STEP.**

***Index Terms*—Adaptive differential protection, current phase angle, microgrid protection, spherical tokamak power plant.**

I. Introduction

THE rapid development of fusion energy has made its interface with electric power systems an important engineering issue. Unlike large-scale concepts such as Europe's demonstration power plant (DEMO) and the U.S. affordable, robust, compact (ARC), the Spherical Tokamak for Energy Production (STEP) program targets comparatively compact commercialization, with the STEP prototype power plant (SPP) designed to export more than 100 MWe to the national grid [1]. Since established protection and coordination practices for fusion plants are not yet available, this first-stage study models the SPP as a DER-based microgrid and adopts differential protection as the baseline to investigate protection challenges arising from hybrid sources and multimode operation.

The SPP combines high-capacity inverter-interfaced distributed generators (IIDGs) and rotating machines, represented by a battery energy storage system (BESS) and a synchronous generator (SG). Their different source dynamics produce mode-dependent fault signatures in both magnitude and phase angle: IIDGs provide limited and controlled fault currents, whereas SGs contribute inertia-driven transient fault currents [2], [3]. In addition, the SPP operates in multiple modes with different source participation, power-flow directions, and fault levels, particularly between grid-connected and islanded operation. As a result, faults at the 3 same location can exhibit different observability and protection requirements across modes [4]. Static differential-protection settings therefore risk underreaching internal faults or maloperation during external disturbances, compromising zone coordination and system reliability.

Considering the challenges presented by the SPP microgrid, conventional differential protection (ANSI 87) is reviewed as the protection baseline. ANSI 87 employs a slope-biased restraint to tolerate current transformer (CT) errors, load imbalance, and inrush currents, and has been extended to feeders and microgrids through communication-assisted implementations. A comprehensive review of differential protection challenges and solutions in IBR-dominated microgrids is provided in [2]. However, conventional slope-biased differential protection may still lose sensitivity under weak-infeed, high-impedance, and mode-dependent fault conditions, especially when inverter-interfaced sources and rotating machines coexist in the same microgrid.

Several enhanced differential protection methods have been proposed to improve sensitivity under weak infeed and inverter-dominated conditions. In [5], a positive-sequence fault component (PSFC)-based current differential scheme replaces phase currents with PSFCs, improving immunity to load flow and enhancing sensitivity; however, its applicability is limited to phase-to-phase and three-phase-to-ground faults. Phase-angle- and phasor-based quantities have also been explored. In [6], two-ended distribution phasor measurement unit (D-PMU) synchrophasors are used to compute the absolute

This work was supported in part by STEP Fusion, a major technology and infrastructure programme led by UKFE, which aims to deliver the UK's prototype fusion power plant and a path to the commercial viability of fusion. The review of this article was arranged by Senior Editor M. Kovari. textit(Corresponding author: Min Zhang.)

Shiyao Yu, Min Zhang, and Qiteng Hong are with the Department of Electronic and Electrical Engineering, University of Strathclyde, G1 1XW Glasgow, U.K. (e-mail: shiyao.yu@strath.ac.uk; min.zhang@strath.ac.uk; q.hong@strath.ac.uk).

Eduardo Sato and Ioannis Antoniou are with the United Kingdom Atomic Energy Authority (UKAEA), Culham Campus, OX14 3DB Oxfordshire, U.K. (e-mail: eduardo.sato@ukaea.uk; ioannis.antoniou@ukaea.uk).

Color versions of one or more figures in this article are available at https://doi.org/10.1109/TPS.2026.3693938.

Digital Object Identifier 10.1109/TPS.2026.3693938

superimposed differential angle (ASDA) of positive-sequence currents. Similarly, [7] proposes a magnitude-phase plane of impedance difference using wide-area positive-sequence currents and voltages for microgrid protection. In [8], the differential negative sequence impedance angle (DNSIA) is employed to detect low- and high-impedance faults, but its effectiveness for symmetrical faults is inherently limited.

Compared with PSFC-based schemes, which depend on sequence fault components and therefore have fault-type applicability limitations, and DNSIA-based schemes, which are more suitable for unbalanced faults than symmetrical faults, the proposed method retains the conventional slope-biased Type 87 framework and superimposes a two-terminal phase-angle supervisory term. Unlike methods relying primarily on sequence-component selectivity, impedance-angle construction, or wide-area voltage and current measurements, the proposed scheme uses the current phasors already available at the terminals of the protected zone. This makes it more suitable for the multisource and multimode SPP microgrid considered in this study. Existing methods remain limited in addressing coordinated protection under high DG penetration, multimode operation, bidirectional power flow, high-resistance faults, and transient disturbances. To address these gaps, this work proposes a phase-angle-superimposed differential scheme with current restraint and mode-dependent adaptive thresholds, and evaluates it on the RTDS/RSCAD platform under representative SPP operating conditions. The main contributions of this work are as follows.

1) A phase-angle-superimposed differential protection scheme is developed to improve the sensitivity of conventional 87 elements under IIDG current limiting and SG excitation/inrush effects.
2) Mode-dependent adaptive thresholds are introduced to maintain protection security under variations in DER output, load profile, and power flow direction.
3) The proposed scheme achieves millisecond-level internal fault detection while preserving restraint under external faults, thereby reducing the exposure of reactor-related components to faults and avoiding maloperation.
4) The method builds on existing ANSI 87 logic by adding only a two-terminal phase-angle supervisory term, thereby limiting additional communication requirements.

The remainder of this article is organized as follows. Section II describes the SPP microgrid architecture and operating modes. Section III formulates the protection problem. Section IV presents the proposed protection scheme. Section V reports the performance evaluation, and Section VI concludes the research findings and outlines future research content.

II. SPP Microgrid System

A. Architecture Overview

The SPP microgrid is a nonconventional, high-voltage, and high-capacity microgrid representing the operational characteristics of a future fusion power plant [1]. Based on the conceptual power infrastructure proposed by U.K. Fusion Energy (UKFE), Fig. 1 shows the source-oriented protection layout and relay allocation across generation and load subsystems. A 400 kV integrated bus interconnects the three principal power sources: the 400-kV utility grid, the BESS branch, and the 11-kV fusion generator, which is represented by an SG to emulate its electromechanical behavior. The BESS is interfaced with the plant AC network through a bidirectional voltage source converter and a step-up transformer, with its converter side represented at 33 kV and its AC connection side at 275 kV. These sources supply the critical fusion loads and the static and hotel loads. For system-level protection studies, critical fusion loads with dedicated converter-based supplies are represented as aggregated plant-level AC load branches, while their internal converter interfaces and DC-side details are not modeled explicitly.

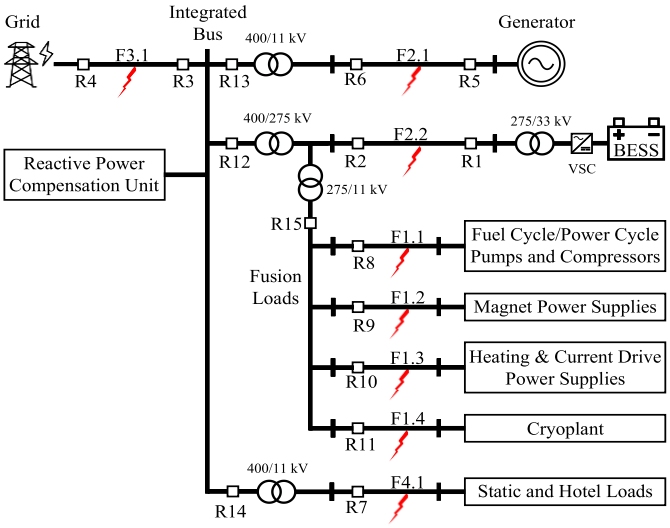

Fig. 1. One-line diagram of SPP microgrid.

The relay architecture includes primary differential relays R1–R6 for the grid, BESS, and SG source feeders, time-coordinated overcurrent relays R7–R11 for the load feeders, and backup directional overcurrent relays R2, R3, R6, and R12–R15 for overreaching protection in the event of primary protection failure. Fault locations F1.1–F4.1 are selected on branches associated with the major subsystems, including the load interfaces, DG terminals, and grid intertie, to support system-level protection coordination analysis. The considered fault resistance ranges from 0.01 to 100 Ω, and the fault types include single-line-to-ground, line-to-line, three-phase, and three-phase-to-ground faults. This arrangement is intended to capture the different fault-current characteristics of inverter-based and rotating sources in the SPP microgrid.

B. Multimode Operational Topologies

To accommodate fusion-driven operational flexibility, the SPP microgrid is represented by several operating modes with different source and load participation. As summarized in Table I, these modes define the connection status and power

TABLE I

REPRESENTATIVE SOURCE AND LOAD PARTICIPATION

	Grid	BESS	SG	Fusion Loads	Static and Hotel loads
Start-up	√+	√+		√	√
Boost-up	√+	√+		√	√
Generating	√-	√-	√+	√	√
Islanded		√-	√+	√	√
Boost-down	√+	√+		√	√
Shutdown	√+	√+		√	√
Standby	√+			√	√

TABLE II

MAIN SETTING PARAMETERS USED IN THE REPORTED CASE STUDIES

Protection branch	Operating mode	I_{pickup} (kA)	k_1	I_{bp} (kA)	k_2	I_{ft} (kA)
SG	Generating	11.50	50%	29.90	165%	135.00
SG	Islanded	7.70	40%	25.35	145%	96.00
BESS	Start-up	0.12	54%	-	-	6.00
BESS	Boost-up	0.12	66%	-	-	7.20
BESS	Generating	0.04	31%	-	-	4.80
BESS	Islanded	0.08	21%	-	-	2.00
Grid	Generating	0.20	99%	0.40	153%	10.00

flow role of the grid interface, BESS, SG, fusion loads, and static and hotel loads. In Table I, "√" indicates connected status, "$\sqrt{}^{+}$" indicates a source connected and supplying power to the microgrid, and "$\sqrt{}^{-}$" indicates a source connected and absorbing power from the system.

The operating modes are defined as follows.

1) *Start-up*: Fusion-related loads and static and hotel loads are energized mainly by the grid and BESS.
2) *Boost-up:* The grid and BESS jointly supply the loads, and plant demand reaches its maximum level.
3) *Generating*: After the plasma reaches a stable state, the SG supplies the plant loads, charges the BESS, and exports surplus power to the grid.
4) *Boost-down:* Generation is reduced while the grid and BESS support the fusion-related loads.
5) *Shutdown*: This mode represents the final controlled transition of an operating cycle, during which plant loads are gradually reduced toward Standby.
6) *Standby*: The plant remains in a demand-reduced state between operating cycles, or between two subsequent pulses, supplied primarily by the grid to keep essential auxiliary loads energized.
7) *Islanded*: When grid disconnection is required, and a complete shutdown is undesirable, the SG supplies local loads autonomously, and the BESS regulates its power to maintain power balance.

The representative power profiles of the SPP operating cycle are illustrated in Fig. 2. The normal operating sequence consists of start-up, boost-up, generating, boost-down, shutdown, and standby, while islanded operation may be introduced during generating, if required. In general, the BESS is discharged during start-up, boost-up, boost-down, and shutdown, and charged in generating and islanded mode.

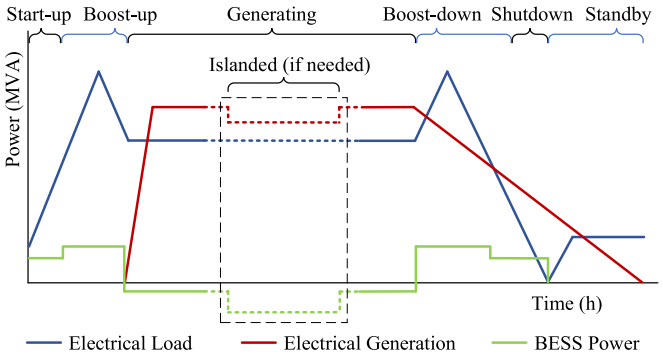

Fig. 2. SPP power profile under the defined operating modes.

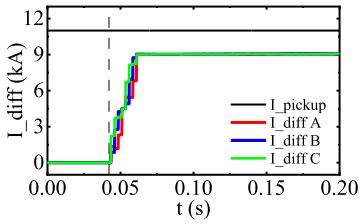

Fig. 3. Three-phase differential current versus pickup threshold.

III. RESEARCH PROBLEM STATEMENT

A. Protection Challenge of Hybrid Power Sources in SPP Microgrid

In the SPP microgrid, the fault current contributions from hybrid sources, particularly the SG and the converter-interfaced BESS branch, are difficult to predict due to their fundamentally different dynamic responses. The BESS converter supplies fault current in a controlled and limited manner, whereas the SG can contribute larger transient currents. As a result, the differential current observed by a protected feeder is strongly dependent on the source participation, power-flow direction, and operating mode. This behavior is especially challenging under high-impedance internal faults, where the fault current may be weak or redistributed among multiple sources.

Conventional slope-biased Type 87 protection relies primarily ON current-magnitude information [9]. Under high-impedance internal faults, the resulting differential current may remain below the operating threshold or within the restraint region, causing the relay to underreach. Fig. 3 illustrates this limitation during a high-impedance internal fault on a protected feeder, the three-phase differential current I_{diff} does not exceed the required operating level I_{pickup}, and no trip signal is issued despite the presence of an internal fault.

When the current differential element underreaches, directional overcurrent protection is commonly used as a backup. However, conventional directional logic relies on a sufficiently clear voltage–current phase relationship to determine the fault direction [10]. In the SPP microgrid, this condition is not always satisfied due to bidirectional power flow, converter current limitations, and multisource fault-current paths. As shown in Fig. 4(a), for a high-impedance internal fault on

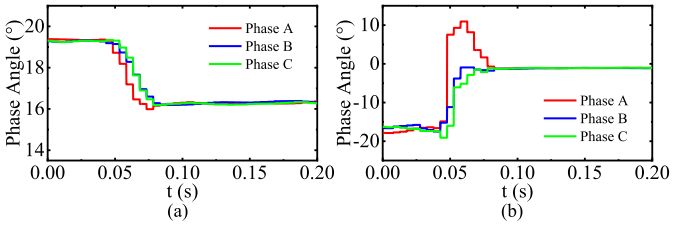

Fig. 4. Phase angle changes of (a) SG and (b) BESS branch.

the SG branch, the voltage–current angular change is small and does not produce a clear directional reversal. Similarly, Fig. 4(b) shows that during BESS charging, the BESS branch may behave as a passive absorbing path, so the current direction does not provide a reliable indication of an internal fault. These cases show that conventional directional backup may also fail to identify internal faults when the current magnitude and directional signatures are both weak or ambiguous.

Therefore, this work introduces a phase-angle-superimposed differential criterion based on the interterminal current phase relationship of the protected zone, together with mode-dependent adaptive thresholds. The purpose is not to replace the conventional Type 87 framework, but to enhance its sensitivity to internal faults that are not sufficiently observable from conventional differential current magnitude or directional logic alone.

B. Impact of Multimode Operation on Coordination

The operating conditions of the system vary significantly across modes, each involving different combinations of active power sources, power flow directions, and even system topology. The relative contributions from the utility grid, SG, and BESS—as well as the instantaneous load profile—directly influence the fault current level and, consequently, the performance requirements for differential protection. Conventional current differential schemes typically rely on static threshold settings, which lack adaptability to these mode-dependent variations. As a result, internal faults may go undetected in low-fault-level scenarios, while external disturbances under high-fault-level conditions may trigger false trips. These limitations severely compromise protection coordination across zones under different modes, posing risks to overall system reliability.

These challenges underscore the need for phase-angle-superimposed fault indicators and mode-dependent adaptive thresholds to ensure reliable fault detection and coordination under hybrid, multimode operation.

IV. Proposed Protection Scheme

A. Overall Scheme Architecture

The proposed protection scheme adopts a two-stage differential protection process, as illustrated in Fig. 5. Three-phase currents are first measured at the relay terminals, and the operating mode is identified through supervisory communication. Based on the identified mode, the corresponding pre-established setting group is then selected to update I_{pickup}, I_{set}, and θ. The measured currents are then processed using

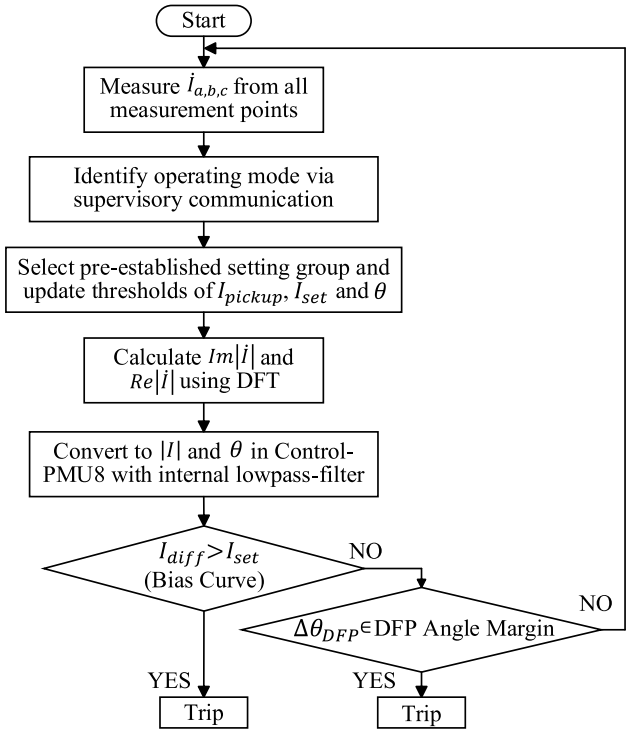

Fig. 5. Flowchart of the proposed protection scheme.

DFT-based phasor extraction, after which the current magnitudes and phase angles are obtained in the control-PMU with internal low-pass filtering. The relay first evaluates the slope-biased differential current criterion. If this element does not operate, a second-stage supervision based on the phase-angle deviation criterion is applied. In this way, the proposed scheme enhances internal-fault detectability under multimode operation while preserving restraint against external faults and reducing the risk of unintended tripping.

B. Phase-Angle-Superimposed Differential Protection

The proposed phase-angle-superimposed criterion complements the conventional 87 differential protection with second harmonic restraint. The phase angles of the three-phase currents at the two ends of the protected zone are continuously compared in real time. For each phase $\theta \in \{a, b, c\}$, the interterminal phase difference is calculated as follows:

$$\Delta\theta_{DFP}(a,b,c) = \angle I_1(a,b,c) - \angle I_2(a,b,c). \tag{1}$$

Under normal operating conditions or external faults, the differential phase-angle $\Delta\theta$ will be close to $\pm 180°$, as currents entering and leaving the protection zone remain nearly antiphase due to throughflow continuity. On the contrary, for internal faults, the interterminal phase difference will deviate significantly from $\pm 180°$, reflecting the loss of current balance within the protected zone. The superimposed tripping condition for differentials is therefore defined as follows:

$$I_{diff} > \begin{cases} I_{pickup} + k_1 \cdot I_{bias}, & I_{bias} \le I_{bp} \\ I_{pickup} + k_1 \cdot I_{bias} + k_2 \cdot (I_{bias} - I_{bp}), & I_{bias} > I_{bp} \end{cases} \tag{2}$$

$$I_{bias} = \frac{|I_1| + |I_2|}{2} \tag{3}$$

$$Max.\,|\Delta\theta_{DFP}\,(a,b,c) - 180°| > \theta_{threshold} \tag{4}$$

where I_{bias} is the restraint current; I_{pickup} is the pickup threshold for initiating the slope-biased differential element; k_1 and k_2 are the low- and high-restraint slope parameters, respectively; and I_{bp} is the breakpoint current on the restraint current axis at which the characteristic changes from k_1 to k_2. I_1 and I_2 are the three-phase currents measured at the two terminals of the protected zone. The phase-angle criterion uses $\theta_{threshold}$ as the allowable deviation margin and is asserted only when the threshold violation persists for at least τ_{min}, which is set to one simulation time step, i.e.,100 μs, to prevent short-duration spurious excursions from causing unintended operation. A trip signal is issued when either the slope-biased current differential criterion is satisfied or the phase-angle-superimposed criterion is asserted. The representative numerical settings used in the reported case studies are summarized in Table II, where I_{ft} is the high-set force tripping current threshold. The implication of this setting under time synchronization mismatch is further illustrated in Section V-D. A dedicated robustness assessment with respect to CT error and saturation is beyond the scope of this study.

C. Adaptive Threshold Setting Strategy

Fixed threshold settings optimized for a single condition will therefore lead to a lack of protection or over-protection in multimode operation. To address this, an adaptive threshold setting strategy is proposed, enabling real-time adjustment of I_{bias} for differential protection according to the prevailing operating state of the microgrid.

1) The operating mode is identified through supervisory communication (e.g., an optical-fiber link) with the microgrid supervisory controller, which provides the real-time status of circuit breakers, source output, and load demand. This supervisory information is used only to determine the prevailing operating mode and to trigger the corresponding selection of the setting group. The mode identification is updated continuously to reflect any changes in system configuration or dispatch schedule.

2) The threshold adjustment logic is based on three inputs.

a) Operating mode, which determines the number and type of active sources.

b) Active power contributions from the grid, SG, and BESS, reflecting the available fault current from each source.

c) Load profile changes, which can alter prefault loading levels and affect fault current margin.

3) The threshold mapping method is that once the operating mode is identified, the protection settings are mapped from a pre-established offline database derived from comprehensive fault analysis. The database stores optimal differential and overcurrent protection setting groups for the representative operating modes and credible fault scenarios considered in this study, including the relevant combinations of fault type, fault resistance, fault location, and system configuration, determined from extensive simulation studies. Within the scope of the work, this database is constructed to be exhaustive for all defined fault scenarios. At runtime, the protection controller selects the corresponding pre-established setting group and applies the associated threshold values; no online optimization of protection settings is performed.

This adaptive threshold mechanism ensures consistent fault detection performance across all modes of operation while minimizing the risk of underreach due to mode-dependent variations in fault current characteristics. The system operator controls the system's operational state via the switcher, at which point the protection threshold is switched to the corresponding threshold setting.

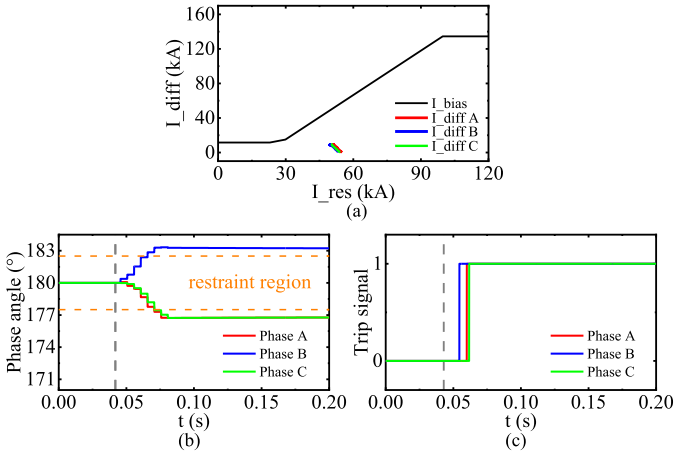

Fig. 6. Case 1 (a) differential current with 87 slope-bias characteristic, (b) differential phase angle, and (c) trip signal.

V. Performance Evaluation

A. Internal Fault in Generating Mode

During generating mode, a 1-Ω three-phase-to-ground internal fault is applied on the SG branch. As shown in Fig. 6(a), the operating point of the conventional 87-element remains entirely below the bias characteristic throughout the event, $I_{op} < I_{pickup}$. Consequently, no trip is issued despite the internal fault in the conventional 87-element. On the contrary, the proposed phase-angle scheme detects a prompt postfault angular excursion that exceeds its preset threshold shown in Fig. 6(b), which drives the tripping signal within 19 ms after fault inception, as illustrated in Fig. 6(c). This case evidences the superior sensitivity of the angle-based logic to high-impedance internal faults that the magnitude-based differential element fails to detect in generating mode.

B. Internal Fault in Islanded Mode

In islanded mode, a 1-Ω line-to-line fault is applied on the SG branch. As shown in Fig. 7(a), although the operating current exceeds the pickup as $I_{op} > I_{pickup}$, the operating point remains in the restraint region so that the conventional 87-element does not trip. On the contrary, the proposed phase-angle scheme registers a prompt postfault angular excursion that surpasses its preset threshold, as shown in Fig. 7(b),

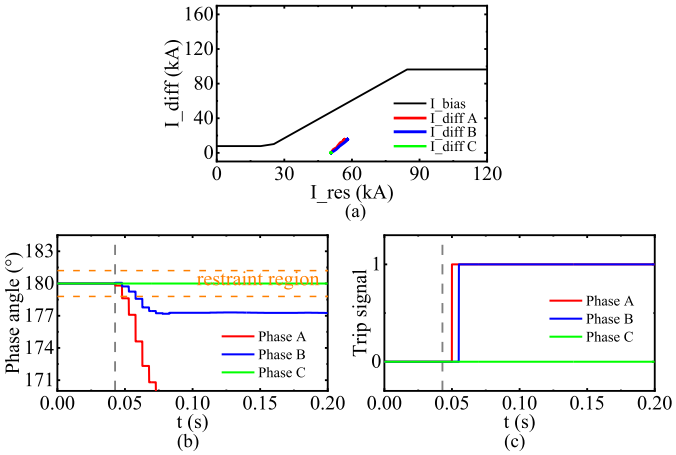

Fig. 7. Case 2 (a) differential current with 87 slope-bias characteristic, (b) differential phase angle, and (c) trip signal.

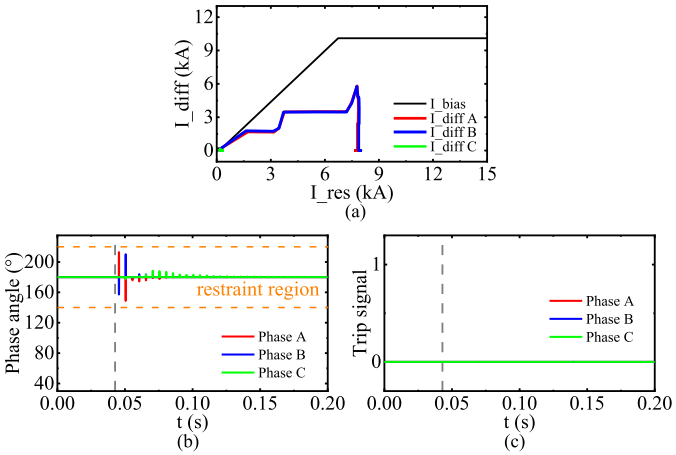

Fig. 8. Case 4 (a) differential current with 87 slope-bias characteristic, (b) differential phase angle, and (c) trip signal.

thereby asserting the tripping signal within 9.6 ms, as shown in Fig. 7(c). The SG branch adopts a comparatively tighter phase-angle threshold because its internal faults generally produce smaller phase-angle deviations than those of the other branches. This case underscores that the angle-based logic retains sensitivity to high-impedance internal faults even when the magnitude-based differential element is restrained by bias.

C. External Fault Sensitivity to Time Synchronization Mismatch

To verify the security of the proposed scheme under the circumstance of 0.2-ms time synchronization mismatch, a representative 10-Ω phase-to-phase external fault located on the BESS branch is applied outside the protected zone of the grid branch relay during generating mode. As shown in Fig. 8(a), the three-phase-differential current operating points remain below the bias characteristic, so the conventional 87-element remains restrained. The phase-angle deviations in Fig. 8(b) also stay within the restraint margin and do not exceed the tripping threshold. Consequently, the proposed scheme issues no trip signal, as shown in Fig. 8(c). This case confirms that the proposed method maintains external

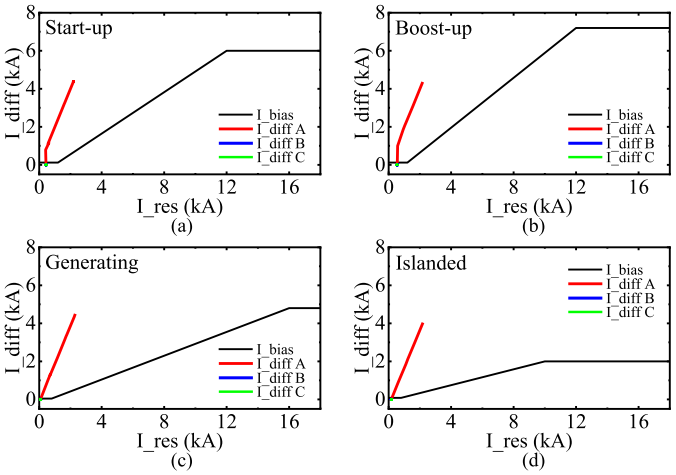

Fig. 9. Case 3 adaptive bias curve of BESS in (a) start-up, (b) boost-up, (c) generating, and (d) islanded mode.

fault security under the modeled synchronization mismatch condition.

D. Adaptive Setting for Multimodes

This case evaluates the adaptive action thresholds, slopes, and overcurrent monitoring performance of the BESS branch on the 275-kV AC side under ideal time synchronization during four operating modes, including start-up, boost-up, generation, and islanded mode. Each subfigure shows mode-specific slope-bias characteristic curves, annotating actual trip currents and suppression currents for the 20 Ω a–g internal fault.

1) *Fig. 9(a) Start-Up*: With limited relative fault contribution, the adaptive setting adopts a higher pickup threshold and a steeper slope to prioritize security; the operating point remains in the trip region.
2) *Fig. 9(b) Boost-Up:* The setting is moderately relaxed to accommodate increased power sharing while maintaining selectivity. The operating point remains above the bias curve, enabling detection of the high-impedance fault.
3) *Fig. 9(c) Generating*: During BESS low-power charging, the reduced and reversed current is addressed by lowering the pickup threshold while retaining sufficient restraint.
4) *Fig. 9(d) Islanded:* Following grid disconnection, the setting provides higher sensitivity with reduced operating thresholds and mode-dependent slopes. The operating point remains clearly in the trip region, providing a sufficient operating margin.

VI. Conclusion

This article reviews prior research on phase-angle-related differential protection and develops a protection scheme tailored to the SPP microgrid, building on the conventional ANSI 87 relay while accounting for its hybrid-source and multimode fault characteristics. The proposed method uses the current phase angle as an auxiliary supervisory criterion to improve

internal-fault detection under the combined influence of IIDGs and rotating machines. The results also show that external-fault restraint is maintained under the tested time synchronization mismatch condition. Furthermore, a mode-dependent adaptive threshold mechanism is introduced to support reliable coordination across multiple operating modes. The scheme is validated on a simplified SPP microgrid model covering seven operating modes, three fault types, and fault resistances ranging from 0.01 to 100 Ω. Compared with conventional differential protection, the proposed scheme identifies the studied internal faults within 3–30 ms, with a worst case operating time of 30 ms for the tested high-impedance fault scenarios, while the conventional Type 87 element fails to detect certain high-impedance internal faults. These results provide preliminary theoretical evidence supporting the future commercialization of STEP. Future work will extend the proposed scheme to nonideal measurement scenarios, including CT saturation and systematic CT errors. It will also investigate the detection of communication loss, latency, and mode-recognition failure, as well as the fail-safe transition from adaptive differential protection to the directional overcurrent backup layer and its detailed coordination logic.

REFERENCES

[1] J. Acres, I. Antoniou, F. Christie, D. Blackburn, and S. Knight, "Staying positive: Producing net power," *Phil. Trans. Roy. Soc. A, Math., Phys. Eng. Sci.*, vol. 382, no. 2280, Oct. 2024, Art. no. 20230404.

[2] S. Sanati, I. Kamwa, B. Cao, B. Sheng, and X. Minghui, "A comprehensive review on differential protection schemes in IBR-dominated microgrids," *IEEE Access*, vol. 12, pp. 170250–170272, 2024, doi: 10.1109/ACCESS.2024.3486061.

[3] W. M. Hamanah, M. I. Hossain, M. Shafiullah, and M. A. Abido, "AC microgrid protection schemes: A comprehensive review," *IEEE Access*, vol. 11, pp. 76842–76868, 2023, doi: 10.1109/ACCESS.2023.3298306.

[4] P. Singh, U. Kumar, N. K. Choudhary, and N. Singh, "Advancements in protection coordination of microgrids: A comprehensive review of protection challenges and mitigation schemes for grid stability," *Protection Control Mod. Power Syst.*, vol. 9, no. 6, pp. 156–183, Nov. 2024, doi: 10.23919/pcmp.2023.000250.

[5] H. Gao, J. Li, and B. Xu, "Principle and implementation of current differential protection in distribution networks with high penetration of DGs," *IEEE Trans. Power Del.*, vol. 32, no. 1, pp. 565–574, Feb. 2017, doi: 10.1109/TPWRD.2016.2628777.

[6] G. S. Dua, F. Sattar, S. K. Sadanandan, and T. Ghaoud, "Evaluating synchrophasor-enabled angle-based differential protection in distribution networks," *Electr. Power Syst. Res.*, vol. 241, Apr. 2025, Art. no. 111261.

[7] N. K. Sharma and S. R. Samantaray, "A composite magnitude-phase plane of impedance difference for microgrid protection using synchrophasor measurements," *IEEE Syst. J.*, vol. 15, no. 3, pp. 4199–4209, Sep. 2021, doi: 10.1109/JSYST.2020.2999483.

[8] K. Dubey and P. Jena, "Impedance angle-based differential protection scheme for microgrid feeders," *IEEE Syst. J.*, vol. 15, no. 3, pp. 3291–3300, Sep. 2021, doi: 10.1109/JSYST.2020.3005645.

[9] D. Costello, "Lessons learned through commissioning and analyzing data from transformer differential installations," in *Proc. 60th Annu. Conf. Protective Relay Eng.*, College Station, TX, USA, Mar. 2007, pp. 341–365, doi: 10.1109/CPRE.2007.359911.

[10] K. Narendra, D. Fedirchuk, N. Zhang, R. Midence, N. Perera, and V. Sood, "Phase angle comparison and differential rate of change methods used for differential protection of busbars and transformers," in *Proc. IEEE Electr. Power Energy Conf.*, Winnipeg, MB, Canada, Oct. 2011, pp. 134–139, doi: 10.1109/EPEC.2011.6070183.